Hang Liu and Li-Qiang Feng*

Selection of Single Harmonic Emission Peak for Producing Isolated Attosecond Pulse via Chirped-UV Combined Field

https://doi.org/10.1515/zna-2019-0220 Received June 28, 2019; accepted September 8, 2019; previously published online September 25, 2019

Abstract: A potential method to produce isolated attosecond pulses (IAPs) by using low-intensity chirped-UV combined field has been investigated. The results can be separated into three parts. First, by properly introducing the mid-chirp or down-chirp of the low-intensity laser field, the harmonic cutoff can be extended and achieve the referenced value, which is produced from the highintensity referenced field. Moreover, the spectral continuum is contributed by a single harmonic emission peak, which is beneficial to produce IAPs. However, the harmonic yield is very low due to the lower driven laser intensity. Second, by properly adding a UV pulse, the harmonic yield can be enhanced and achieve the referenced value due to the UV resonance ionisation. The intensity of the combined field is lower than that of the referenced field, which reduces the experimental requirements for producing high-intensity spectral continuum. Third, with the introduction of the positive or negative inhomogeneous effect of the mid-chirped combined field or down-chirped combined field, respectively, the similar harmonic cutoff and harmonic yield can also be obtained but with a much lower driven laser intensity. Finally, by superposing the harmonics on the spectral continuum, the IAPs with the durations of sub-38 as can be obtained.

Keywords: Chirped Pulse; High-Order Harmonic Generation; Inhomogeneous Effect of Laser Field; Isolated Attosecond Pulse; Single Harmonic Emission Peak

PACS: 42.65.Ky; 42.65.Re; 32.80.Fb

1 Introduction

Coherent extreme ultraviolet (XUV) pulse is an important tool for some potential applications. There are several ways to generate XUV pulse, and one of the approaches to produce coherent XUV pulse is high-order harmonic generation (HHG), which was first observed in neon gas by McPherson et al. [1] in 1987. Currently, the HHG can be produced from atoms, molecules, and solids [2–5]. However, the generation of isolated attosecond pulses (IAPs) is mainly produced by superposition of spectral continuum from atomic system.

The HHG from atomic system can be explained by Schafer et al. [6] and Corkum [7] in 1993. They explained the HHG in term of a three-step model. First step: atoms of gas are ionised due to interaction of the intense laser field with atom. Second step: the ionised electron is accelerated in the laser field and gains energy. Third step: if the electron recombines with its parent ion, it emits its energy as high photon energy. According to the three-step model, the harmonic cutoff is proportional to the laser intensity (I) and inversely proportional to the square of the laser frequency (ω^2). Finally, a harmonic cutoff with the value of $I_p + 3.17 U_p (U_p \sim I/\omega^2)$ can be obtained. Generally, to obtain the high-intensity XUV pulse in attosecond scale, three requirements are needed. First, a broad spectral continuum in XUV region is needed. Second, the enough intense harmonic yield is required. Third, the spectral continuum should be contributed by a single harmonic emission peak (HEP). On the basis of the three-step model, a number of methods have been proposed to achieve the above three requirements and to produce the coherent attosecond XUV pulse, such as increasing the laser intensity or shape of the optical profile by using a multicolour combined field (including IR, MIR, and UV fields) [8-15], chirped pulses [16-21], inhomogeneous field [22-27], and polarisation gating technology [28-31].

In most of the above investigations, the main purpose is to extend the harmonic cutoff and to produce the attosecond pulse with the higher photon energy. Thus, usually, a high-intensity fundamental laser field is needed to largely extend the harmonic cutoff in XUV or X-ray

^{*}Corresponding author: Li-Qiang Feng, Laboratory of Molecular Reaction Dynamics, Liaoning University of Technology, Jinzhou 121001, China, E-mail: lqfeng_lngy@126.com

Hang Liu: Laboratory of Molecular Reaction Dynamics, Liaoning University of Technology, Jinzhou 121001, China

regions. However, the high intensity is not very easy to obtain in experiment.

Therefore, in this article, we propose a potential method to obtain a high-intensity spectral continuum by using a low-intensity chirped combined field. It is shown that with the optimisation of the low-intensity chirped-UV combined field (including mid-chirped-UV combined field and down-chirped-UV combined field) the harmonic cutoff and the harmonic yield can achieve the referenced values, which are obtained from a high-intensity referenced field. Moreover, the spectral continuum is contributed by a single HEP. Further, if the positive or negative inhomogeneous effect of the mid-chirped combined field or downchirped combined field is introduced, respectively, much lower laser intensity is needed to achieve the referenced values of the harmonic cutoff and harmonic yield. Finally, by properly superposing the harmonics on the spectral continuum, the IAPs shorter than 38 as can be produced. It should be noted that the intensity of the combined field is lower than that of the referenced field, which reduces the experimental requirements for producing high-intensity spectral continuum and IAPs.

2 Methods

In order to study the HHG process of atoms, it is necessary to numerically solve the time-dependent Schrödinger equation (TDSE). In the single active electron approximation and dipole approximation, the TDSE under the length-gauge is given by [32-36]

$$i\frac{\partial \psi(x,t)}{\partial t} = \left[-\frac{1}{2} \frac{\mathrm{d}^2}{\mathrm{d}x^2} + V(x) + x \cdot E(x,t) \right] \psi(x,t),\tag{1}$$

where $V(x) = -1/\sqrt{0.484 + x^2}$ is the soft Coulomb potential of He. E(x, t) is laser field, which is given by

$$\begin{split} E(x,t) &= [1+g(x)]E_1 \exp[-4\ln(2)(t)^2/\tau_1^2]\cos(\omega_1 t + \delta(t)) \\ &+ E_2 \exp[-4\ln(2)(t-t_{\rm delay})^2/\tau_2^2]\cos(\omega_2 (t-t_{\rm delay})), \end{split} \tag{2}$$

Here, g(x) means the inhomogeneous form, and it is quite different for different fields and geometrical shapes of nanostructure [23, 27]. In this article, we use only the first-order approximation of the inhomogeneous form, and it can be expressed as g(x) = cx. c is the inhomogeneous parameter with c = 0, c > 0, and c < 0, meaning the homogeneous field, positive inhomogeneous field, and negative inhomogeneous field, respectively. E_i , ω_i , and τ_i (i = 1, 2) are the amplitudes, frequencies, and durations of two laser fields, respectively. $t_{\rm delay}$ is the time delay of the two pulses. $\delta(t)$ is the chirp form of the fundamental laser field. Particularly, $\delta(t) =$ $\beta_1 \tanh(t/400)$ [16, 21, 37] means the mid-chirped pulse, and $\delta(t) =$ $\beta_2 \omega_1 t^2$ ($\beta_2 < 0$) [19, 21] means the down-chirped pulse, respectively. It should be emphasised that the recent advancement in optical parametric amplification and optical parametric chirped-pulse amplification technology has made it possible to perform coherent wavelength multiplexing of ultra-broadband pulses with full phase and amplitude control, thus allowing the generation of any optical waveform

[38–41]. That is to say, the specific waveform used in this article can be obtained in the laboratory. In the present calculations, the maximum radius of the partial waves is chosen to be |x| = 800 a.u., and the grid spacing of the radius is chosen to be dx = 0.1 a.u. The TDSE can be integrated numerically by adopting the second-order splitoperator method with time spacing of dt = 0.2 a.u. [42]. Moreover, a mask function with the form cos1/8 was used to avoid the wave packet near the boundaries that contribute to the HHG.

Taking the Fourier transform of the time-dependent dipole acceleration a(t) and taking the modulus squared, we can acquire the HHG power spectrum $S(\omega)$:

$$S(\omega) = \left| \frac{1}{\sqrt{2\pi}} \int a(t)e^{-i\omega t} dt \right|^2, \tag{3}$$

where $a(t) = \langle \psi(x, t) | - \frac{\partial V(x)}{\partial x} + \frac{\partial (xE(x,t))}{\partial x} | \psi(x, t) \rangle$.

To analyse the temporal structures of HHG, the time-frequency analyses of HHG can be expressed as [37, 43]

$$A_{\omega}(t_0, \omega_0) = \int a(t) w_{t_0, \omega}(t) dt. \tag{4}$$

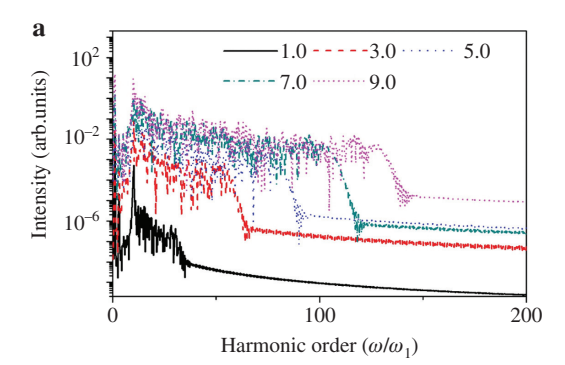
Here, $w_{t_0,\omega}(t)$ is the wavelet transform kernel, which can be expressed as $w_{t_0,\omega}(t)=\sqrt{\omega}W[\omega(t-t_0)]$ where the kernel of the wavelet is $W(x) = \frac{1}{\sqrt{\alpha}} e^{ix} e^{-x^2/2\alpha}$. By superposing several harmonics, the IAPs can be produced:

$$I_{\text{IAP}}(t) = \left| \sum_{q} a_q e^{iq\omega t} \right|^2, \tag{5}$$

where $a_q = \int a(t)e^{-iq\omega t}dt$.

3 Results and Discussion

Before our discussion, we first choose a referenced harmonic cutoff and harmonic yield produced from a referenced field. Here, the laser field is chosen to be 10 fs-800 nm homogeneous field (c = 0) with laser intensity changing from $I_1 = 1.0 \times 10^{14} \text{ W/cm}^2$ to $I_1 = 1.0 \times 10^{15} \text{ W/cm}^2$. The HHG spectra are shown in Figure 1a. As can be seen, the harmonic cutoff can be enhanced as the laser intensity increases. However, the harmonic yield is first enhanced and then decreased as the laser intensity increases. And a maximum harmonic yield around $I_1 = 7.0 \times 10^{14} \text{ W/cm}^2$ can be found. According to three-step model, the HHG yield is relative to the ionisation probability and the occupancy of ground state. Thus, the enhancement of the HHG yield is attributed to the increase of ionisation probability, while the decrease of the HHG yield is because of the depletion of ground state [44]. Therefore, we choose the harmonic cutoff (103rd order) and harmonic yield (0.007) from $I_1 = 7.0 \times 10^{14} \text{ W/cm}^2$ as the referenced values and $I_1 = 7.0 \times 10^{14} \text{ W/cm}^2$ as the referenced laser intensity. Figure 1b shows the timefrequency analyses of HHG driven by the above referenced field. We see that the signal of the HHG spectrum is coming



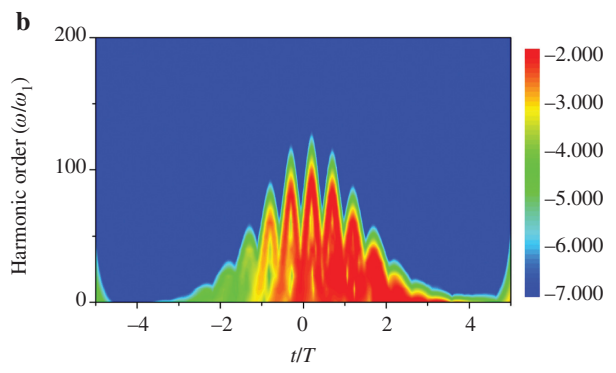


Figure 1: The harmonic emission process. (a) The HHG spectra driven by the 10 fs-800 nm pulse with laser intensity being 1.0, 3.0, 5.0, 7.0, and 9.0 \times 10¹⁴ W/cm². (b) The timefrequency analyses of HHG driven by the 10 fs-800 nm pulse with $I_1 = 7.0 \times 10^{14} \text{ W/cm}^2$.

from the couple of multi-HEPs, which is unbeneficial to the generation of IAPs. Thus, in the following discussion, we try to use a low-intensity combined field to obtain the similar harmonic cutoff and harmonic yield as those produced from the referenced field. Moreover, the signal of spectral continuum should be contributed by a single HEP.

3.1 Extension of Harmonic Cutoff and Selection of Single HEP by Using a **Low-Intensity Homogeneous Chirped Pulse**

As discussed before, the frequency-chirping technique is an important method to extend the harmonic cutoff (due to the harmonic cutoff is proportional to $1/\omega^2$). Thus, in this part, we try to use the low-intensity chirped pulse to extend the harmonic cutoff and achieve the referenced value. The chirp forms are chosen to be $\delta(t)$ = $\beta_1 \tanh(t/400)$ (mid-chirped pulse) and $\delta(t) = \beta_2 \omega_1 t^2$ (for down-chirped pulse), respectively. The laser field is still 10 fs-800 nm pulse, but with the laser intensity being 1.0×10^{14} W/cm². Figure 2a shows the HHG spectra driven by the low-intensity mid-chirped pulse and downchirped pulse. The chirp parameters are $\beta_1 = -7.4$ and $\beta_2 = -0.004$, respectively. Clearly, by properly introducing the chirps of the laser field, the harmonic cutoffs from the low-intensity chirped pulses can achieve the referenced value. However, because of the lower driven laser intensity, the HHG yield is much lower than that from the referenced field. Figure 2b-d show the laser fields and the time-frequency analyses of HHG for the cases of low-intensity chirp-free and mid-chirped pulses. It is found that with the introduction of mid-chirp the instantaneous frequency on the middle part of the laser field is decreased, as shown in Figure 2b and c. According to threestep model, the harmonic cutoff is proportional to $1/\omega^2$. Thus, the decrease of instantaneous frequency on the middle part of the laser field leads to the extension of HEP of PA, as shown in Figure 2d. This is the reason behind the harmonic cutoff extension for adding the mid-chirped pulse. Figure 2e and f show the laser fields and the timefrequency analyses of HHG for the cases of low-intensity down-chirped pulse. As can be seen, the introduced downchirp leads to the decrease of instantaneous frequency on the falling part of the laser field (Fig. 2e). Thus, the ionised electron will receive more energy during its acceleration in this region, which leads to the extension of HEP of P_B, as shown in Figure 2f. This is the reason behind the harmonic cutoff extension for adding the down-chirped pulse. Furthermore, compared with the harmonic emission process between chirp-free pulse and chirped pulses, we see that the signal of spectral continuum is contributed by a single HEP for the chirped pulses, while it is contributed by the couple of multi-HEPs for the chirp-free pulse. Thus, the chirped pulse (including both mid-chirp and down-chirp) is much better for selecting the single HEP and producing IAPs. However, the intensity of spectral continuum is still lower than the referenced value. Thus, in the next part, we try to enhance the HHG yield.

3.2 Enhancement of Harmonic Yield by **Using UV Resonance Ionisation Scheme**

As discussed before, the HHG yield is sensitive to the ionisation probability. Thus, to enhance the HHG yield, many schemes have been proposed, such as the pumpprobe two-colour field scheme [45, 46], the superposition of initial state scheme [47, 48], the use of Rydberg state [49, 50], and the UV resonance ionisation scheme [51, 52]. In this part, we use the UV resonance ionisation scheme to enhance the HHG yield. The advantage of this scheme is that a weaker laser field can be used to improve the

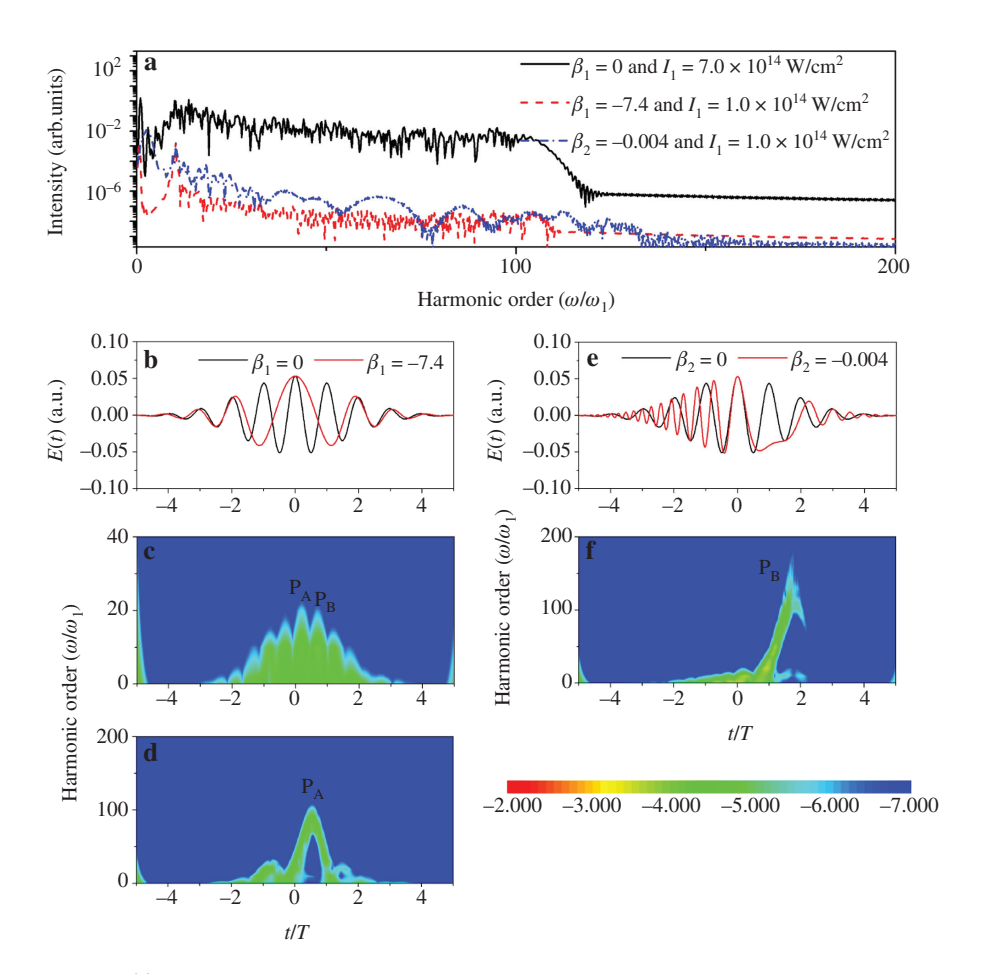


Figure 2: (a) The HHG spectra driven by the low-intensity mid-chirped pulse and down-chirped pulse. The chirp parameters are $\beta_1 = -7.4$ and $\beta_2 = -0.004$, respectively. The laser field is still 10 fs-800 nm pulse but with the laser intensity being 1.0 \times 10¹⁴ W/cm². (b-d) The laser fields and the time-frequency analyses of HHG for the cases of low-intensity chirp-free and mid-chirped pulses. (e and f) The laser fields and the time-frequency analyses of HHG for the cases of low-intensity down-chirped pulse.

HHG yield, which is just what we want in this article. Here, the UV laser pulse is chosen to be 1.45 fs-123 nm pulse (10 optical cycles). The reason for choosing this UV pulse is because its photon energy approximately equals the double-photon resonance transition between the ground state and first excited state of He atom. Figure 3a shows the HHG yield as a function of UV laser intensity. The chirp form is chosen to be mid-chirped pulse. The delay time of the two pulses is $t_{\rm delay} = -1.0T$, where T is the optical cycle of 800 nm pulse. Clearly, as the UV pulse is added, the HHG yield can be enhanced. Moreover, when the UV laser intensity is chosen to be $I_2 = 1.8 \times 10^{14} \text{ W/cm}^2$, the HHG yield from the combined field reaches the referenced value. Figure 3b shows the HHG spectra from the referenced field, the single mid-chirped pulse, and the combined field. Clearly, with the introduction of the UV pulse, not only that the HHG yield can be enhanced, but also the modulation on the HHG spectrum is reduced, which is beneficial to IAP generation. Figure 3c-e show the laser

fields, the ionisation probabilities, and the time-frequency analyses of HHG driven by the mid-chirped combined field. As can be seen, when the UV pulse is introduced, due to the effect of UV resonance ionisation, the ionisation probability at t > -1.0T can be remarkably increased compared with that from the single mid-chirped pulse (Fig. 3d). That is to say, much more electron can be ionised around t = -1.0T point and accelerated in the following half waveform region, thus leading to the enhancement of PA, as shown in Figure 3e. This is the reason behind the intensity enhancement of spectral continuum. Moreover, when the harmonics are larger than the 30th order, the harmonic spectrum is only contributed by PA, which is responsible for the smaller modulation on the spectral continuum. As can be seen, with the combination of the mid-chirped pulse and UV pulse, the referenced harmonic cutoff and harmonic yield can be obtained. Moreover, the spectral continuum is contributed by a single HEP. Most importantly, the total intensity of the mid-chirped

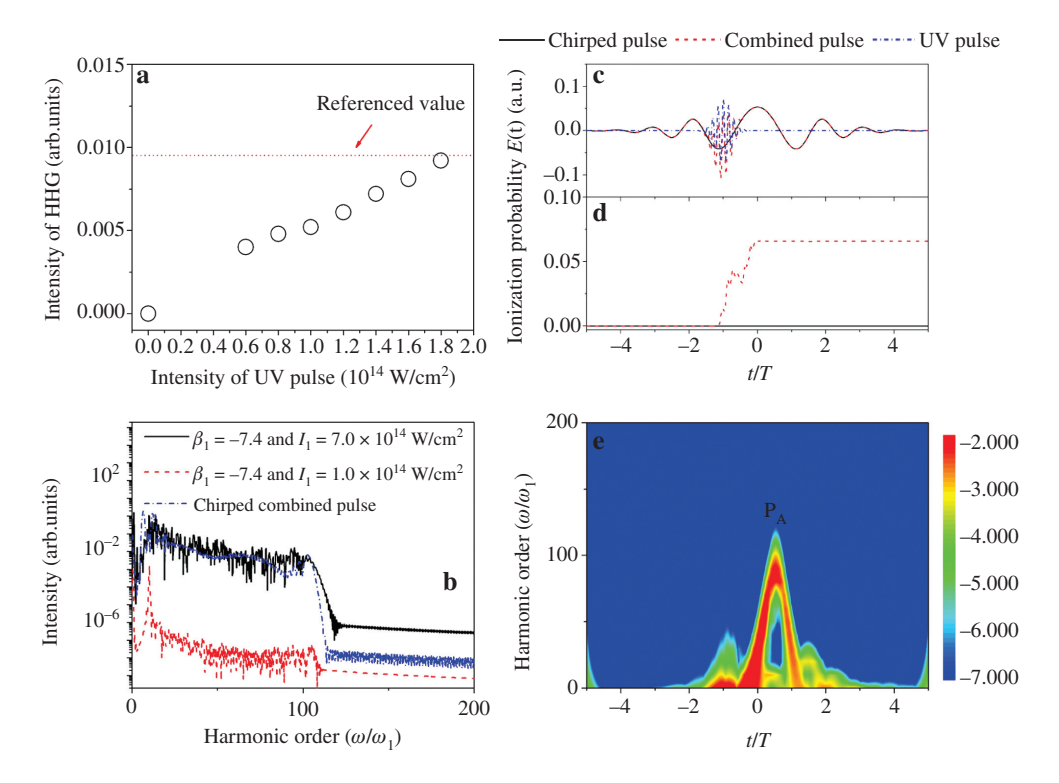


Figure 3: (a) The HHG yield as a function of UV laser intensity. The chirp form is chosen to be mid-chirped pulse. The delay time of the two pulses is $t_{\text{delay}} = -1.07$, where T is the optical cycle of 800 nm pulse. (b) The HHG spectra from the referenced field, the single mid-chirped pulse, and the combined field. (c-e) The laser fields, the ionisation probabilities, and the time-frequency analyses of HHG driven by the mid-chirped combined field.

combined field (1.0 \times 10¹⁴ W/cm² + 1.8 \times 10¹⁴ W/cm² = $2.8 \times 10^{14} \text{ W/cm}^2$) is lower than that of the referenced field $(7.0 \times 10^{14} \text{ W/cm}^2)$. This will reduce the experimental requirements for obtaining high-intensity spectral continuum.

Figure 4a shows the HHG yield as a function of UV laser intensity. The chirp form is chosen to be down-chirped pulse. The delay time of the two pulses is $t_{\rm delay} = -0.2T$. It is shown that the HHG yield can also be enhanced as the UV laser intensity increases. Moreover, when the UV laser intensity is chosen to be $I_2 = 1.4 \times 10^{14} \text{ W/cm}^2$, the HHG yield from the combined field can achieve the referenced value. Figure 4b shows the HHG spectra from the referenced field, the single down-chirped pulse, and the combined field. Similar as that in the mid-chirped combined field, not only that the HHG yield from the combined field can be enhanced, but also the modulation on the HHG spectrum is reduced. Figure 4c-e show the laser fields, the ionisation probabilities, and the time-frequency analyses of HHG driven by the down-chirped combined field. We see that due to the UV resonance ionisation the ionisation probability at t = -0.2T can be remarkably increased (Fig. 4c), which leads to the remarkable enhancement of P_B and is responsible for the harmonic yield improvement (Fig. 4e). Moreover, the spectral continuum from the 30th order to the 110th order is only coming from P_B, which is the reason behind the smaller modulation on the spectral continuum. Furthermore, the total intensity of down-chirped combined field (1.0 \times 10¹⁴ W/cm² + 1.4 \times 10¹⁴ W/cm² = $2.4 \times 10^{14} \text{ W/cm}^2$) is also lower than that of the referenced field (7.0 \times 10¹⁴ W/cm²), which meet our requirements.

3.3 Generation of Referenced Harmonic **Cutoff and Harmonic Yield from Much** Lower Inhomogeneous Chirped Combined Field

According to recent investigations [22–27, 53–55], we know that the spatial inhomogeneous field can remarkably reduce the laser intensity requirement for HHG. This is because the intensity of the inhomogeneous field will be increased as spatial extension. Thus, in this part, we try to obtain the referenced harmonic cutoff and harmonic yield from a much weaker inhomogeneous combined field. Generally, for the symmetric inhomogeneous laser field, the laser intensity can be increased along both positive

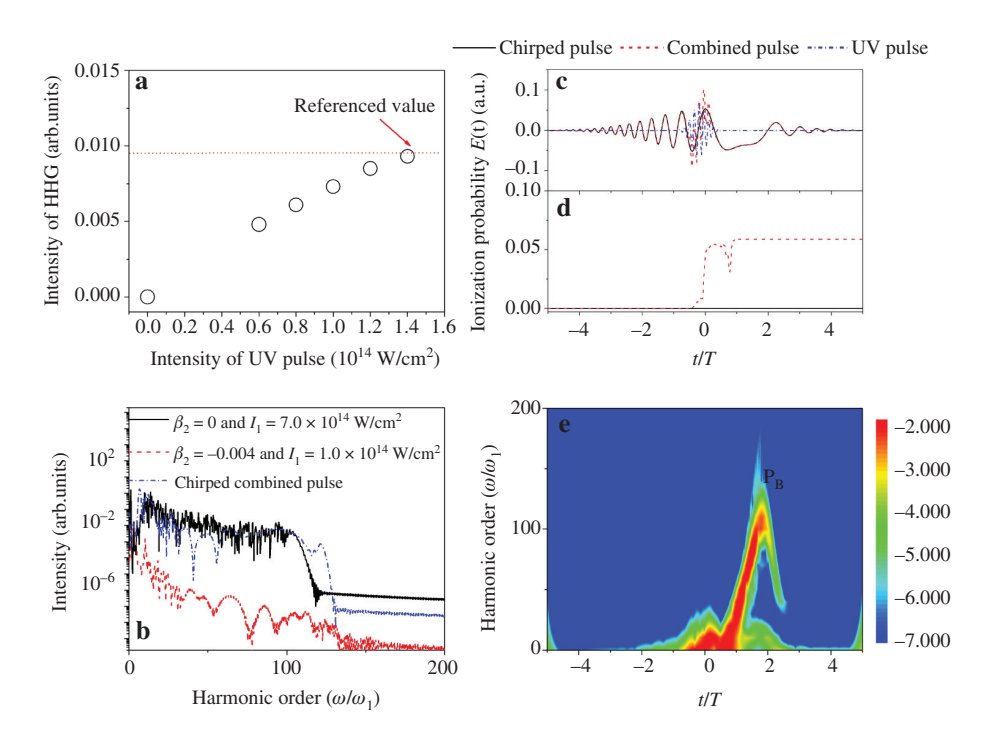


Figure 4: (a) The HHG yield as a function of UV laser intensity. The chirp form is chosen to be down-chirped pulse. The delay time of the two pulses is $t_{\text{delav}} = -0.27$. (b) The HHG spectra from the referenced field, the single down-chirped pulse, and the combined field. (c-e) The laser fields, the ionisation probabilities, and the time-frequency analyses of HHG driven by the down-chirped combined field.

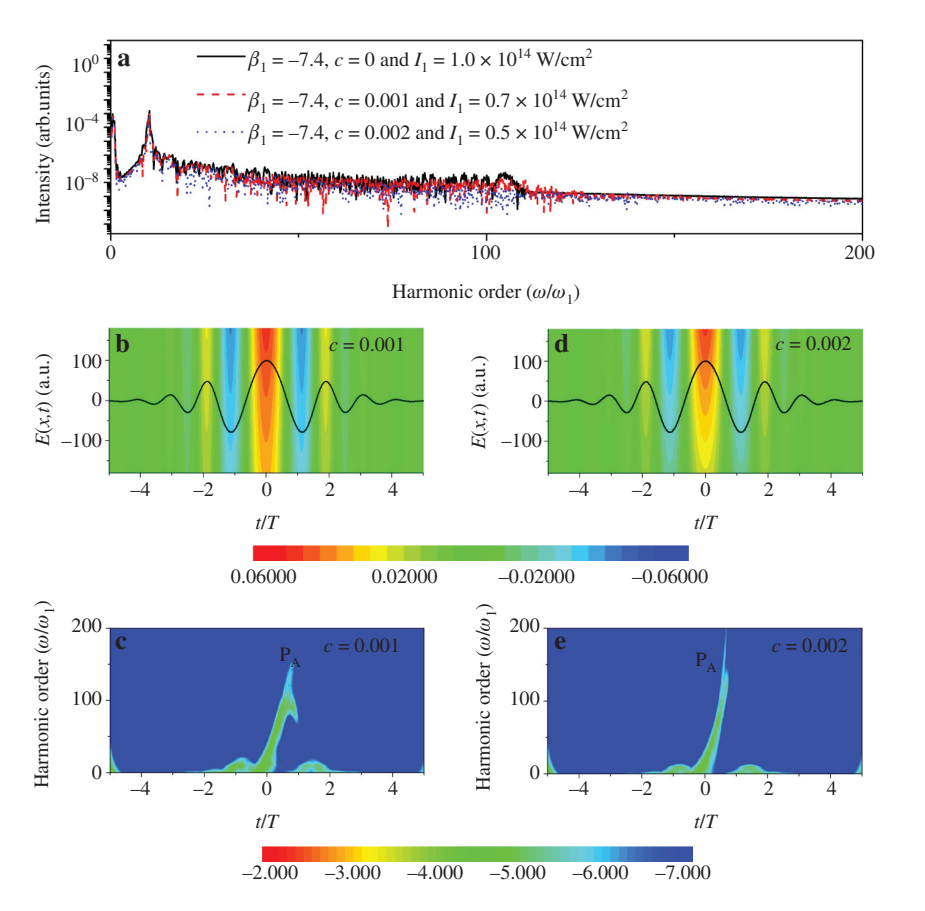


Figure 5: (a) The HHG spectra driven by the positive inhomogeneous mid-chirped pulse. The laser fields in time and space and the time-frequency analyses of HHG driven by the positive inhomogeneous mid-chirped pulse with (b, c) c = 0.001 and (d, e) c = 0.002.

-7.000

and negative directions, thus leading to the extension of the harmonic cutoff from both E(t) > 0 and E(t) < 0 [55], while for the asymmetric inhomogeneous laser field, the laser intensity can be increased only along positive or negative direction, which leads to the extension of the harmonic cutoff from E(t) > 0 (for positive asymmetric inhomogeneous laser field) or E(t) < 0 (for negative asymmetric inhomogeneous laser field) [55]. Through analysing the harmonic emission process shown in Figure 2, we see that the spectral continua, caused by PA and PB for the mid-chirped pulse and down-chirped pulse, are coming from E(t) > 0 and E(t) < 0 regions, respectively. Thus, the further extension of the harmonic cutoff is better to choose the positive or negative asymmetric inhomogeneous laser field for the cases of mid-chirped pulse or down-chirped pulse, respectively.

Figure 5a shows the HHG spectra driven by the positive inhomogeneous mid-chirped pulse. The laser parameters are unchanged except for the inhomogeneous parameter and laser intensity. As can be seen, with the introduction of the positive inhomogeneous effect, the referenced harmonic cutoff can be obtained with a lower laser intensity. Moreover, the larger inhomogeneous effect is, the lower laser intensity is needed. For instance, when c = 0.001, the required laser intensity is $I_1 = 0.7 \times 10^{14} \text{ W/cm}^2$, while when c = 0.002, the required laser intensity is only $I_1 = 0.5 \times 10^{14}$ W/cm². Figure 5b-e show the laser fields in time and space and the time-frequency analyses of HHG driven by the positive inhomogeneous mid-chirped pulse. As can be seen in Figure 5b and d, when the positive inhomogeneous effect is introduced, the laser intensity along positive x direction can be enhanced. As a result, when the free electron is accelerated along positive x direction, it will receive more energy compared with that from the homogeneous field, which leads to the extension of HEP coming from E(t) > 0. For the case of mid-chirped pulse, the HEP of P_A is coming from E(t) > 0; thus, it can be extended, as shown in Figure 5c and e. This is the reason behind the lower required laser intensity for the harmonic cutoff extension when using inhomogeneous field. Moreover, the larger laser enhancement can be obtained as the inhomogeneous effect increases, which is responsible for the much lower laser intensity required when the larger inhomogeneous effect is introduced.

Figure 6a shows the HHG spectra driven by the positive inhomogeneous mid-chirped pulse and the positive inhomogeneous mid-chirped pulse combined with the 1.45 fs-123 nm UV pulse. The inhomogeneous parameter is c = 0.002; the laser intensities of mid-chirped pulse and UV pulse are $I_1 = 0.5 \times 10^{14} \text{ W/cm}^2$ and $I_2 = 1.4 \times 10^{14} \text{ W/cm}^2$, respectively. The delay time of two

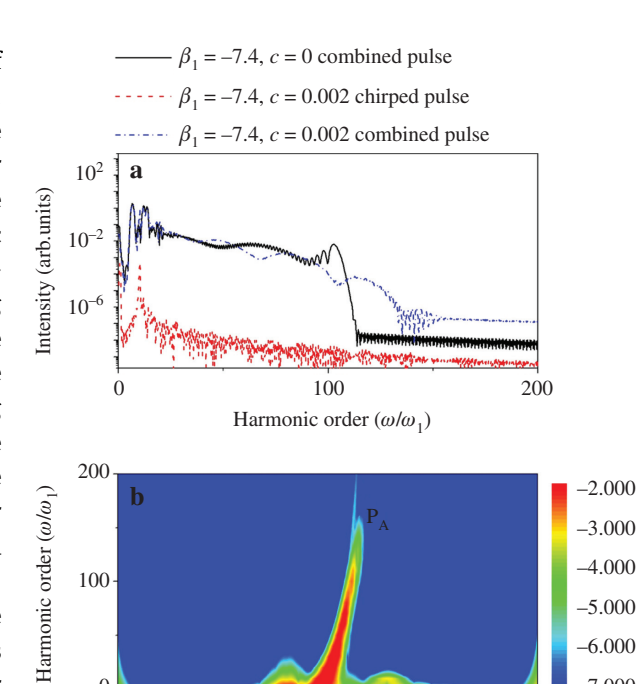


Figure 6: (a) The HHG spectra driven by the positive inhomogeneous mid-chirped pulse and the positive inhomogeneous midchirped pulse combined with the 1.45 fs-123 nm UV pulse. The inhomogeneous parameter is c = 0.002; the laser intensities of mid-chirped pulse and UV pulse are $I_1 = 0.5 \times 10^{14} \text{ W/cm}^2$ and $I_2 = 1.4 \times 10^{14} \text{ W/cm}^2$, respectively. The delay time of two pulses is $t_{\rm delay} = -1.07$. (b) The time-frequency analyses of HHG driven by the above inhomogeneous combined field.

0

t/T

-4

pulses is $t_{\rm delay} = -1.0T$. Similarly as discussed before, the HHG yield can be enhanced as UV pulse is introduced. However, the total laser intensity of the inhomogeneous combined field (0.5 \times 10¹⁴ W/cm² + 1.4 \times 10¹⁴ W/cm² = $1.9 \times 10^{14} \text{ W/cm}^2$) is much lower than that of the homogeneous combined field $(1.0 \times 10^{14} \text{ W/cm}^2 +$ $1.8 \times 10^{14} \text{ W/cm}^2 = 2.8 \times 10^{14} \text{ W/cm}^2$). Figure 6b shows the time-frequency analyses of HHG driven by the inhomogeneous combined field. Clearly, when the harmonics are larger than the 30th order, the spectral continuum is only coming from PA, which meets our requirements and is favourable to generate IAPs.

Figure 7a shows the HHG spectra driven by the negative inhomogeneous down-chirped pulse. The laser parameters are unchanged except for the inhomogeneous parameter and laser intensity. It is found that the harmonic cutoff can be extended and achieve the referenced value when the much weaker negative inhomogeneous downchirped pulse is added. For instance, when c = -0.001, the required laser intensity is $I_1 = 0.8 \times 10^{14} \text{ W/cm}^2$, while when c = -0.002, the required laser intensity is

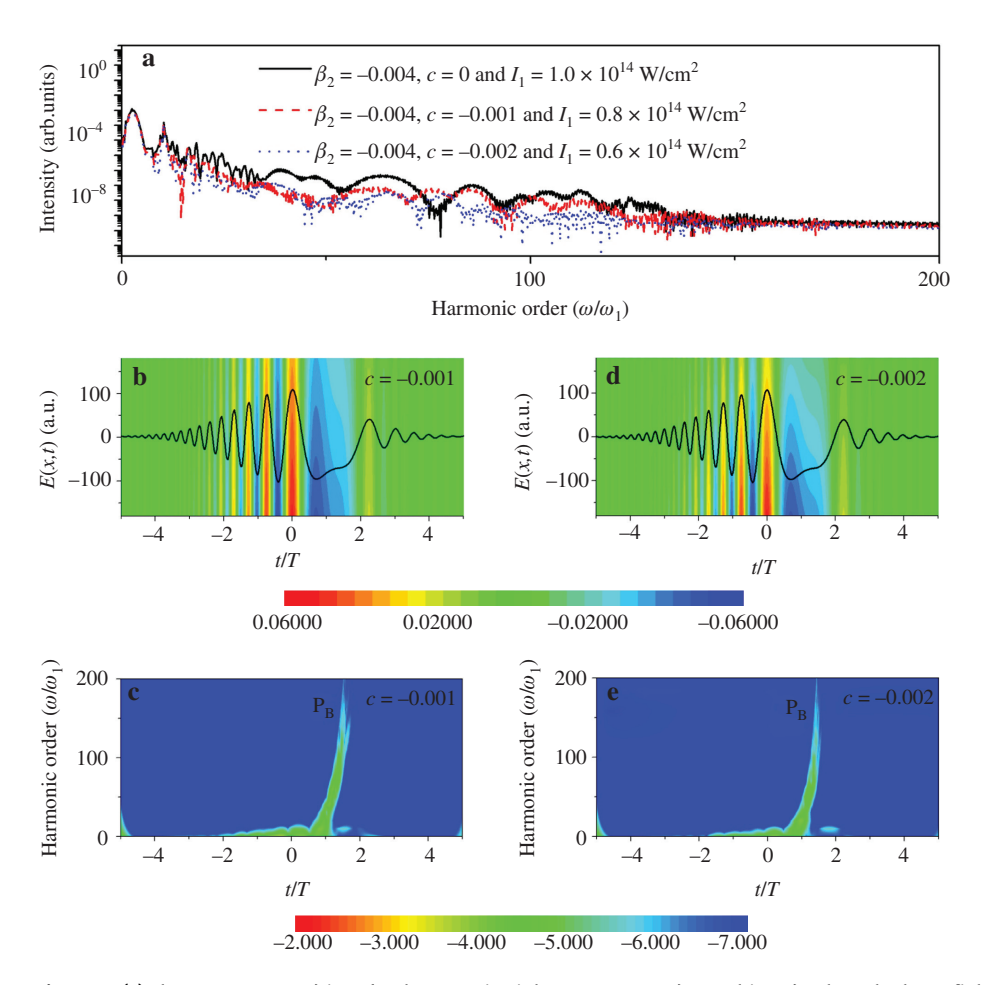


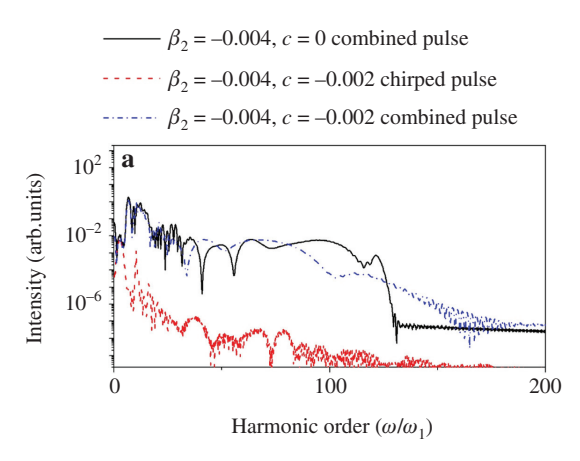
Figure 7: (a) The HHG spectra driven by the negative inhomogeneous down-chirped pulse. The laser fields in time and space and the time-frequency analyses of HHG driven by the negative inhomogeneous down-chirped pulse with (b, c) c = -0.001 and (d, e) c = -0.002.

only $I_1 = 0.6 \times 10^{14}$ W/cm². Figure 7b–e show the laser fields in time and space and the time-frequency analyses of HHG driven by the negative inhomogeneous down-chirped pulse. Through analysing the laser profiles shown in Figure 7b and d, we see that the laser intensity along negative x direction can be increased when the negative inhomogeneous effect is introduced. Thus, the free electron will obtain more energy when it is accelerated along negative x direction, which leads to the extension of HEP coming from E(t) < 0 compared with that from the homogeneous field. For the case of down-chirped pulse, we see that the HEP of P_B is coming from E(t) < 0; thus, it can be extended, as shown in Figure 7c and e, and it is responsible for the harmonic cutoff extension when using a lower intensity inhomogeneous field.

Figure 8a shows the HHG spectra driven by the negative inhomogeneous down-chirped pulse and the negative inhomogeneous down-chirped pulse combined with the 1.45 fs–123 nm UV pulse. The inhomogeneous parameter is c=-0.002; the laser intensities of down-chirped pulse and UV pulse are $I_1=0.6\times10^{14}$ W/cm²

and $I_2=1.0\times10^{14}$ W/cm², respectively. The delay time of two pulses is $t_{\rm delay}=-0.2T$. Clearly, the intensity of spectral continuum from the negative inhomogeneous combined field can also be enhanced and achieve the referenced value. Moreover, the total laser intensity of the inhomogeneous combined field $(0.6\times10^{14} \text{ W/cm}^2+1.0\times10^{14} \text{ W/cm}^2=1.6\times10^{14} \text{ W/cm}^2)$ is still lower than that of the homogeneous combined field $(1.0\times10^{14} \text{ W/cm}^2+1.4\times10^{14} \text{ W/cm}^2=2.4\times10^{14} \text{ W/cm}^2)$. Figure 8b shows the time-frequency analyses of HHG driven by the inhomogeneous combined field. As can be seen, there is only one HEP contributed to the spectral continuum, which is favourable to generate IAPs.

Through the above investigation, we see that by properly using the chirped-UV combined field, the single HEP can be selected to contribute to the spectra continuum. Moreover, the total laser intensity of the combined field is lower than that of the referenced field. Especially when the inhomogeneous effect of the laser field is introduced, much lower laser intensity is needed to achieve



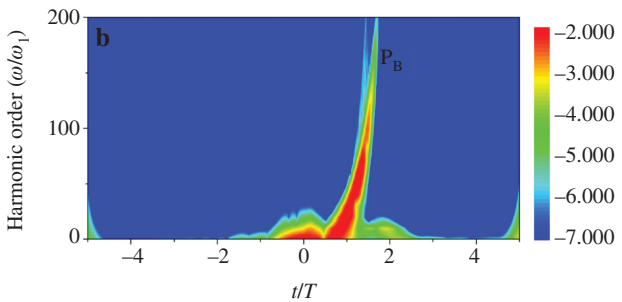
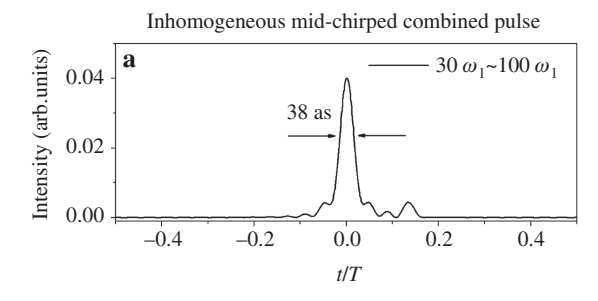


Figure 8: (a) The HHG spectra driven by the negative inhomogeneous down-chirped pulse and the negative inhomogeneous down-chirped pulse combined with the 1.45 fs–123 nm UV pulse. The inhomogeneous parameter is c=-0.002; the laser intensities of down-chirped pulse and UV pulse are $I_1=0.6\times10^{14}~\rm W/cm^2$ and $I_2=1.0\times10^{14}~\rm W/cm^2$, respectively. The delay time of two pulses is $t_{\rm delay}=-0.2T$. (b) The time-frequency analyses of HHG driven by the above inhomogeneous combined field.



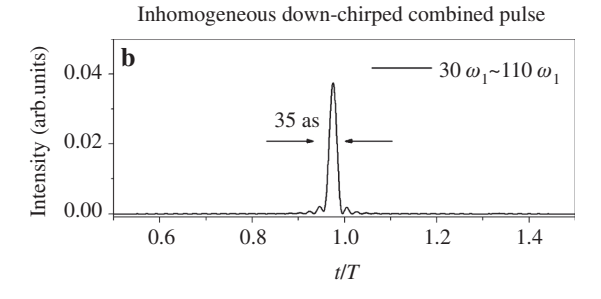


Figure 9: The temporal profiles of IAPs by superposing the harmonics for the case of (a) positive inhomogeneous mid-chirped combined field and (b) negative inhomogeneous down-chirped combined field.

the referenced harmonic cutoff and harmonic yield. Here, we choose the above positive inhomogeneous mid-chirped combined field with c=0.002 and negative inhomogeneous down-chirped combined field with c=-0.002 as the proper conditions. Then, by properly superposing the harmonics on their spectral continua (i.e. from the $30^{\rm th}$ order to $100^{\rm th}$ order for positive inhomogeneous mid-chirped combined field and from the $30^{\rm th}$ order to $110^{\rm th}$ order for negative inhomogeneous down-chirped combined field), two IAPs with durations of 38 and 35 as can be obtained, respectively, as shown in Figure 9a and b.

4 Conclusion

We propose a potential method to obtain the high-intensity spectral continuum by using a low-intensity chirped combined field. We found that by properly using the chirped-UV combined field, not only that the harmonic cutoff and harmonic yield can achieve the referenced values, but also the signal of spectral continuum is contributed by a single HEP. Most importantly, the total laser intensity of the combined field is lower than that of the referenced field. Moreover, as the inhomogeneous effect is introduced, much lower laser intensity is needed to achieve the referenced harmonic cutoff and harmonic yield. Finally, by properly superposing the harmonics on the spectral continuum, two IAPs shorter than 38 as can be obtained. The present scheme reduces the experimental requirements for producing intense IAPs.

Acknowledgements: This work was supported by the National Natural Science Foundation of China (Funder Id: http://dx.doi.org/10.13039/501100001809, no. 11504151), the Liaoning Natural Science Foundation (no. 2019-MS-167), and the Scientific Research Foundation of Liaoning Provincial Education Department, China (JJL201915405).

References

- A. McPherson, G. Gibson, H. Jara, U. Johann, T. S. Luk, et al., J. Opt. Soc. Am. B 4, 595 (1987).
- [2] F. Krausz and M. Ivanov, Rev. Mod. Phys. 81, 163 (2009).
- [3] S. C. Jiang, J. G. Chen, H. Wei, C. Yu, R. F. Lu, et al., Phys. Rev. Lett. **120**, 253201 (2018).
- [4] C. Yu, S. C. Jiang, and R. F. Lu, Adv. Phys. X 4, 1562982 (2018).
- [5] K. J. Yuan and A. D. Bandrauk, Phys. Rev. Lett. 110, 023003 (2013).
- [6] K. Schafer, B. Yang, L. F. DiMauro, and K. C. Kulander, Phys. Rev. Lett. 70, 1599 (1993).
- [7] P. B. Corkum, Phys. Rev. Lett. 71, 1994 (1993).

- [8] C. Jin, G. L. Wang, H. Wei, A. T. Le, and C. D. Lin, Nat. Commun. 5, 4003 (2014).
- [9] H. Liu and L. Q. Feng, Z. Naturforsch. A 72, 941 (2017).
- [10] G. T. Zhang, Z. Naturforsch. A 69, 673 (2014).
- [11] Y. Li, R. L. Q. Feng, and Y. Qiao, Can. J. Phys. DOI: 10.1139/cjp-2019-0002
- [12] X. L. Ge, C. L. Xia, and X. S. Liu, Laser Phys. 22, 1704 (2012).
- [13] L. Li, M. Zheng, R. L. Q. Feng, and Y. Qiao, Int. J. Mod. Phys. B 33, 1950130 (2019).
- [14] R. F. Lu, H. X. He, Y. H. Guo, and K. L. Han, J. Phys. B-At. Mol. Opt. Phys. 42, 225601 (2009).
- [15] L. Q. Feng, Y. B. Duan, and T. S. Chu, Ann. Phys. (Berlin) 525, 915 (2013).
- [16] L. Q. Feng and T. S. Chu, Phys. Rev. A 84, 053853 (2011).
- [17] H. Yuan, L. Fang, and L. Hua, J. Opt. Soc. Am. B 34, 2390 (2017).
- [18] J. J. Carrera and S. I. Chu, Phys. Rev. A 75, 033807 (2007).
- [19] D. Peng, M. V. Frolov, L. W. Pi, and A. F. Starace, Phys. Rev. A 97, 053414 (2018).
- [20] Y. Li, L. Q. Feng, and Y. Qiao, Z. Naturforsch. A 74, 561 (2019).
- [21] E. Neyra, F. Videla, J. A. Pérez-Hernandez, M. Ciappina, L. Roso, et al., Eur. Phys. J. D 70, 243 (2016).
- [22] S. Kim, J. Jin, Y. J. Kim, I. Y. Park, Y. Kim, et al., Nature 453, 757 (2008).
- [23] M. F. Ciappina, J. A. Pérez-Hernández, A. S. Landsman, W. Okell, S. Zherebtsov, et al., Rep. Prog. Phys. 80, 054401 (2017).
- [24] I. Yavuz, M. F. Ciappina, A. Chacón, Z. Altun, M. F. Kling, et al., Phys. Rev. A 93, 033404 (2016).
- [25] C. Yu, H. X. He, Y. H. Wang, Q. Shi, Y. D. Zhang, et al., J. Phys. B-At. Mol. Opt. Phys. 47, 055601 (2014).
- [26] L. O. Feng, Phys. Rev. A 92, 053832 (2015).
- [27] E. Neyra, F. Videla, M. F. Ciappina, J. A. Pérez-Hernandez, L. Roso, et al., J. Opt. 20, 034002 (2018).
- [28] G. Sansone, E. Benedetti, F. Calegari, C. Vozzi, L. Avaldi, et al., Science 314, 443 (2006).
- [29] K. Zhao, Q. Zhang, M. Chini, Y. Wu, X. W. Wang, et al., Opt. Lett. 37, 3891 (2012).
- [30] Q. B. Zhang, P. X. Lu, P. F. Lan, W. Y. Hong, and Z. Y. Yang, Opt. Express 16, 9795 (2008).
- [31] H. Mashiko, S. Gibertson, C. Q. Li, S. D. Khan, M. M. Shakya, et al., Phys. Rev. Lett. 100, 103906 (2008).
- [32] R. F. Lu, P. Y. Zhang, and K. L. Han, Phys. Rev. E 77, 066701 (2008).

- [33] J. Hu, K. L. Han, and G. Z. He, Phys. Rev. Lett. 95, 123001 (2005).
- [34] L. Q. Feng, R. S. Castle, and Y. Li, Mod. Phys. Lett. B 31, 1750282 (2017).
- [35] H. Liu and A. Y. Feng, Z. Naturforsch. A 73, 985 (2018).
- [36] T. S. Chu, Y. Zhang, and K. L. Han, Int. Rev. Phys. Chem. 25, 201 (2006).
- [37] J. X. Han, J. Wang, Y. Qiao, A. H. Liu, F. M. Guo, et al., Opt. Express 27, 8768 (2019).
- [38] P. Wei, J. Miao, Z. N. Zeng, C. Li, X. C. Ge, et al., Phys. Rev. Lett. 110, 233903 (2013).
- [39] E. J. Takahashi, P. Lan, O. D. Mücke, Y. Nabekawa, and K. Midorikawa, Phys. Rev. Lett. 104, 233901 (2010).
- [40] E. J. Takahashi, P. F. Lan, O. D. Mücke, Y. Nabekawa, and K. Midorikawa, Nat. Commun. 4, 2691 (2013).
- [41] L. X. He, Q. B. Zhang, P. F. Lan, W. Cao, X. Zhu, et al., Nat. Commun. 9, 1108 (2018).
- [42] O. Sharafeddin and J. Z. H. Zhang, Chem. Phys. Lett. 204, 190 (1993).
- [43] P. Antoine, B. Piraux, and A. Maquet, Phys. Rev. A 51, R1750 (1995).
- [44] V. V. Strelkov, A. F. Sterjantov, N. Y. Shubin, and V. T. Platonenko, J. Phys. B-At. Mol. Opt. Phys. 39, 577 (2006).
- [45] B. N. Wang, L. X. He, F. Wang, H. Yuan, X. S. Zhu, et al., Opt. Express 25, 17777 (2017).
- [46] L. Q. Feng, Y. Li, and A. Y. Feng, Laser Phys. Lett. 15, 115301 (2018)
- [47] G. T. Zhang and X. S. Liu, J. Phys. B-At. Mol. Opt. Phys. 42, 125603 (2009).
- [48] L. Q. Feng and T. S. Chu, Phys. Lett. A 376, 1523 (2012).
- [49] Z. Zhai, Q. Zhu, J. Chen, Z. C. Yan, P. Fu, et al., Phys. Rev. A 83, 043409 (2011).
- [50] Y. Tikman, I. Yavuz, M. F. Ciappina, A. Chacón, Z. Altun, et al., Pgts. Rev. A 93, 023410 (2016).
- [51] L. Q. Feng and T. S. Chu, IEEE J. Quantum Electron. 48, 1462 (2012).
- [52] P. C. Li, X. X. Zhou, G. L. Wang, and Z. X. Zhao, Phys. Rev. A 80, 053825 (2009).
- [53] I. Y. Park, S. Kim, J. Choi, D. H. Lee, Y. J. Kin, et al., Nat. Photonics 5, 677 (2011).
- [54] J. H. Luo, Y. Li, Z. Wang, Q. B. Zhang, and P. X. Lu, J. Phys. B-At. Mol. Opt. Phys. 46, 145602 (2013).
- [55] L. Q. Feng, W. L. Li, and H. Liu, Ann. Phys. (Berlin) 529, 1700093 (2017).